AIAA JOURNAL
Vol. 38, No. 7, July 2000

Diode Laser Sensor for Gasdynamic Measurements in a Model Scramjet Combustor

B. L. Upschulte,* M. F. Miller,* and M. G. Allen*
Physical Sciences, Inc., Andover, Massachusetts 01810

A sensor for simultaneous and continuous measurements of water vapor density, temperature, and velocity has been developed based on absorption techniques using room temperature diode lasers (InGaAsP) operating at 1.31 θm. Laboratory calibrations of density and temperature were acquired in a variable temperature absorption cell and on a H_2–air flat flame burner from 500 to 2200 K. Laboratory determinations showed absolute accuracies of 5% in temperature and 10% in molecular density for a 0.3-Hz bandwidth. An optical system was developed for integrating the sensor to a model scramjet combustor at the U.S. Air Force Research Laboratory, Wright–Patterson Air Force Base. Preliminary measurements in the Mach 2.1 flowfield at expanded temperatures of 540, 650, and 740 K across an 18-cm pathlength resulted in temperature measurements that agreed with theoretical predictions to within 7–11%. Density measurements agreed with predictions to within 17–56%. Velocity measurement precision was compromised by beam steering effects, although results in reasonable agreement with predictions were observed at the lowest enthalpy condition.

Introduction

CONTINUOUS measurements of in-stream data for gasdynamic and chemical processes are required for development and optimization of advanced propulsion systems. In the case of scramjet engines, measurements of such data are complicated by the high enthalpy of the gas streams. Intrusive probes either do not survive or introduce unacceptable flow disturbances.[1,2] The ultimate objective of ground testing is to measure the net thrust produced by the propulsion system. Especially in scramjet engines, the net thrust provided by the engine is often a relatively small increase in the momentum flux ρV^2 between large inlet and exhaust values. Thus, gasdynamic-based thrust determinations require a sensitive technique capable of simultaneous measurements of gas stream density, velocity, and temperature in high-enthalpy flows.

Optical sensors and diagnostics for combustion flow analysis have received considerable attention during the previous decade because of their inherently nonintrusive nature and their ability to probe relevant species such as O_2, CO, CO_2, NO, OH, and H_2O (Refs. 3 and 4). Laser-based optical techniques for measurements in high-enthalpy flows have undergone extensive development.[3–6] Many of the optical diagnostics have the added value of flowfield mapping using planar imaging techniques[5–9] or high-speed line-of-sight absorption/emission monitoring.[10–18] The latter have been recently reviewed in Ref. 15.

Room temperature distributed feedback (DFB) diode lasers operating at 1.31 μm, originally developed for the telecommunications industry, coincidentally overlap with weak absorption transitions of the $2\nu_3$ and $\nu_1 + \nu_3$ overtone bands of water vapor. Considering the relatively high levels of water vapor expected in combustion facilities, these standard wavelength lasers deserve careful evaluation of their capability to perform diagnostic measurements. Advantages of these lasers include 1) their widespread availability, 2) their excellent single-mode behavior for spectroscopic measurements (i.e., a bandwidth of less than 10 MHz and current tuning ranges of more than 1.5 cm^{-1}), 3) their packaging into ruggedized fiber pigtailed mounts, and 4) their decreasing cost to performance ratio with time as the telecommunication market demand continues to increase.

This work reports continuous simultaneous measurements of water vapor density, temperature, and velocity using room temperature DFB diode lasers operating at 1.31 μm in both laboratory facilities and a model scramjet combustor at the U.S. Air Force Research Laboratory, Wright–Patterson Air Force Base. A stand-alone computer-controlled instrument package was assembled. Two lasers were time multiplexed to measure selected water vapor absorption transitions. A fiber optic network was assembled to combine the outputs from the two diode lasers onto a dual-beam launch and collection system. Below 1200 K, the sensor temperature and density measurements were calibrated in the laboratory, using a high-temperature absorption cell filled with pure water vapor. Above 1200 K, the sensor temperature measurement was calibrated using a H_2–air flat flame burner equipped with a thermocouple corrected for radiation loading. In the flame, the sensor water density measurement was calibrated using chemical equilibrium modeling of the conditions in the flat flame burner with known mass flows of reactants. Integration optics using water cooling and window purge gas flows were specifically developed for the field tests on the model scramjet combustor. Testing new instrumentation in practical ground-based facilities is often limited due to short test times.[16–18] The U.S. Air Force test facility, in contrast, provides a long-duration high-enthalpy flow that is well suited for testing new instrumentation and for developing meaningful statistical information regarding the sensor's performance.[19]

Experimental Approach

The approach for the simultaneous measurement of water vapor density, temperature, and velocity using diode laser absorption techniques is shown schematically in Fig. 1. Radiation from two diode lasers probing different water absorptions is propagated across the sample volume at two different angles. The lasers are frequency scanned to acquire data across the entire absorption lineshape. The two laser wavelengths are multiplexed onto common propagation paths, using a time-domain-multiplexing mode developed by our group and described in an earlier publication.[12] The resultant signals from the balanced ratiometric detector (BRD)[20,21] units are shown schematically in Fig. 2.

The density of water is determined by the integrated area of any of the four absorption lineshapes and spectroscopic constants that depend only on temperature. The temperature is determined by the ratio of the integrated area of two different absorption lines. The flow velocity is determined by the relative Doppler shift in an absorption peak measured at two different angles to the flow vector. The formulas for determination of these parameters are given subsequently. They have been derived and described in detail previously.[12,13]

Briefly, the density is determined from the formula

$$N = \left\{ \int \alpha \, \mathrm{d}\nu \right\} \Big/ [S(T)L] \tag{1}$$

Received 8 April 1999; revision received 22 November 1999; accepted for publication 1 December 1999.

*Principal Research Scientist, 20 New England Business Center.

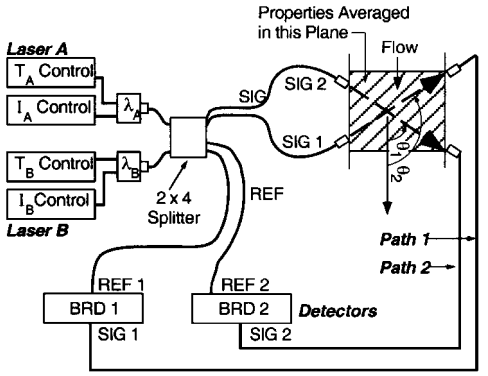

Fig. 1 Schematic layout of simultaneous density, temperature, and velocity measurement system.

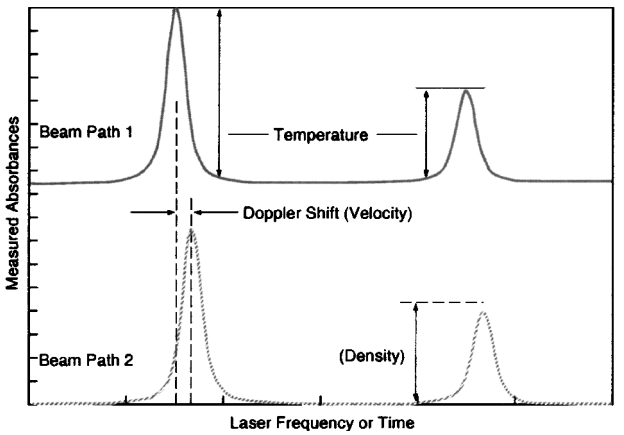

Fig. 2 Signal analysis for simultaneous density, temperature, and velocity measurements.

where α is the absorbance ($-\ln[I_\nu/I_{\nu 0}]$), where I_ν and $I_{\nu 0}$ are the laser intensities after and before propagation through the absorbing gas; the integral is across the entire lineshape; $S(T)$ is the linestrength of the absorption transition; and L is the pathlength.

The temperature is determined from the formula

$$\frac{1}{T} = \frac{1}{T_{\text{ref}}} - \left(\frac{k}{hc\Delta E}\right) \cdot \ln\left\{\left(\int \alpha_1 \, d\nu \Big/ \int \alpha_2 \, d\nu\right) \Big/ \left(\frac{S_1(T_{\text{ref}})}{S_2(T_{\text{ref}})}\right)\right\} \tag{2}$$

where T_{ref} is a reference temperature (normally 298 K); k, h, and c are Boltzmann's constant, Planck's constant, and the speed of light, respectively; the integrals are over each spectral lineshape; $S_1(T_{\text{ref}})$ and $S_2(T_{\text{ref}})$ are the linestrength values at the reference temperature; and ΔE is the energy difference between the lower state energy of each absorption transition.

The velocity is determined from the formula

$$V = c\Delta\nu_{12}/[\nu_0(\cos\theta_1 - \cos\theta_2)] \tag{3}$$

where c is the speed of light, $\Delta\nu_{12}$ is the frequency shift between the lineshapes propagated at angles θ_1 and θ_2 relative to the flow vector, and ν_0 is the center frequency of the transition.

The temperature is most precisely measured using one set of absorption lines for the temperature range from 500 to 1100 K and a second set of absorption lines for the temperature range from 1100 to 2000 K. Analysis of the preceding formula shows that the temperature resolution decreases with increasing temperature, but increases with increasing separation, ΔE, in the lower-state energy levels of the two transitions.[12] Changing absorption transitions to increase ΔE at high-temperature conditions, thus, allows more precise temperature measurements. Spectroscopic parameters[22–24] of the selected transitions are presented in Table 1.

Table 1 Spectroscopic parameters for the selected water transitions

Center frequency ν_0, cm^{-1}	E'', cm^{-1}	v''–v'[a]	ϕ''–ϕ'[b]
Low_{T1}			
7612.0273	285.42	000–002	3,3,0–4,4,1
7612.2682	285.42	000–002	3,3,1–4,4,0
Low_{T2}, 7632.0931	1538.15	000–101	10,3,7–11,5,6
$High_{T1}$, 7605.7967	1201.92	000–101	9,2,7–10,4,6
$High_{T2}$, 7622.7[c]	~8821	Unknown	Unknown

[a] Vibrational quantum number. [b] Rotational quantum number.
[c] Absorption measurements on the transition at 7622.7 cm^{-1} have been analyzed to give an approximate E'' level of 8821 cm^{-1}, but this transition is not assigned by either the HITRAN 98[22] or HITEMP[23] databases.

Sensor Calibration

Because the overtone transitions near 1.31 μm are weak, little spectroscopic information is available for them, particularly at high temperatures. Therefore, it was necessary to calibrate the sensor and to develop the underlying spectroscopic database. Low-temperature calibrations were performed in a temperature-controlled cell and have been published in Ref. 24. Linestrength and collisional broadening measurements in this cell were compared with HITRAN[22] and HITEMP predictions.[23] High-temperature calibrations were performed in a well-characterized Henken-type flat flame burner.[25] The experimental setup of the burner optics consisted of f/2 spherical mirrors arranged in a Herriott geometry.[26] An entrance slot and an exit slot in the mirrors allow access for the laser beam fiber optic launch and BRD signal detector. The mirrors were mounted on two-dimensional micrometers for x–y positioning and on two-axis gimbal mounts for control of the reflection pattern and total pathlength through the flame. Measurements were performed using 28 passes over the flame, for a total in-flame pathlength of 71 cm. The total pathlength was verified by measuring the entrance and exit power of the laser and comparing to the known reflectivity of the mirrors at 1.31 μm. The pathlength in the flame is calculated using the ratio of the linear dimension of the burner surface to the mirror separation. The nitrogen shroud flow surrounding the burner is velocity-matched to the combustion exhaust gases so that the gradient in both temperature and H_2O number density at the interface is within a few millimeters at the measurement height. Although edge effects can be significant in some applications, we do not believe that they constitute a significant source of error or uncertainty in the present work because we have had generally excellent agreement between similar optical measurements and other published data for temperature and composition in past studies.[4, 12, 25]

For water density and temperature calibrations, the burner was fueled with technical grade H_2 without further purification. Flows of all gases were regulated with precision needle valves and measured with mass flow meters. Flows of nitrogen and oxygen in a 80:20 ratio simulated air for the burner. Nitrogen flow was metered into the shroud region of the burner to prevent entrainment of humid room air into the flow of combustion gases. Nitrogen is also metered into a purge region outside the combustion/shroud to eliminate absorption from ambient humidity in the optical absorption path through the laboratory air and to prevent condensation on the mirrors.

Flame measurements were preceded by simulations, using a chemical equilibrium code (STANJAN) to predict water mole fractions at the flame gas temperature measured with a radiation corrected thermocouple. Measurements were performed with equivalence ratios ranging from 0.2 to 1.0, corresponding to temperatures of 900 to 2000 K. An infrared (IR) viewer was used to confirm ignition, flamelet stability, and overall flame shape. At the lowest equivalence ratios, we observed that not all of the individual flamelets of the burner ignited, leading to potentially larger uncertainty in the equilibrium assumption.

A radiation corrected Pt/Pt–13% Rh thermocouple was used to measure the postcombustion gas temperature. The radiation correction for the 0.25-mm bead ranged from 20 K at 1000 K to about 170 K at 2000 K (Refs. 27 and 28). Figure 3 presents a summary of measured and calculated flame temperatures. Temperature profiles at several heights and across both dimensions of the flame indicated

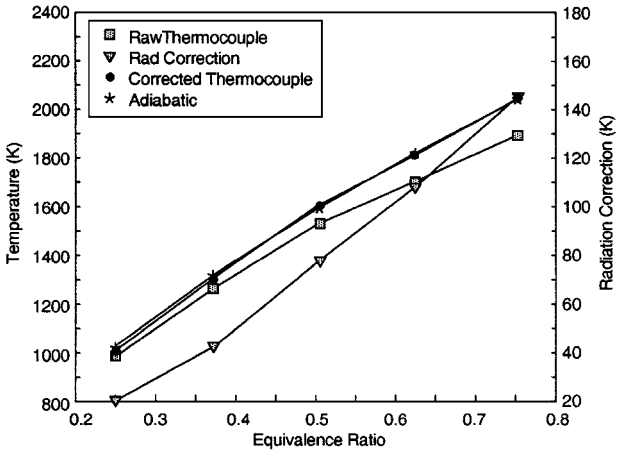

Fig. 3 Flat flame burner temperature measurements as a function of H_2–air equivalence ratio using a thermocouple.

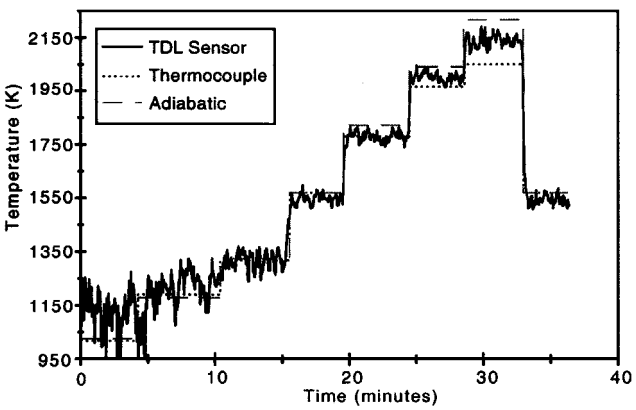

Fig. 4 Comparison of optical temperature measurements to thermocouple and adiabatic values for various flame stoichiometries.

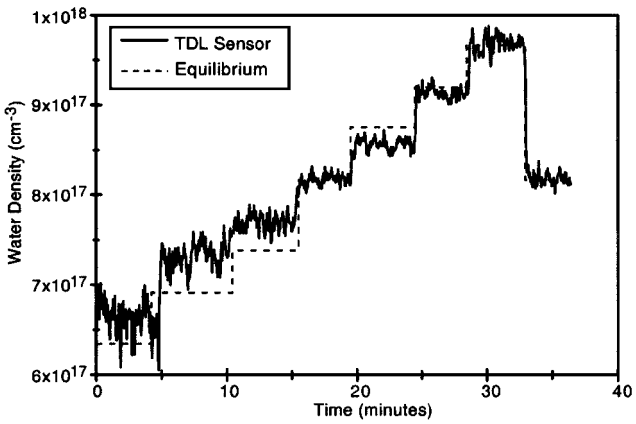

Fig. 5 Comparison of optical water vapor density measurements to predicted equilibrium values for various flame stoichiometries.

the flame profile is sharply defined with a horizontal dimension of 26 mm.

Measurements in the flat flame burner involved recording both water density and temperature with the diode laser sensor simultaneously with thermocouple measurements as the equivalence ratio is changed in discrete steps. Figures 4 and 5 show the results from one sequence. The absolute temperature accuracy is always better than 100 K, and in most cases the measurement precision is ±15 K. Small discrepancies between the thermocouple and adiabatic temperatures in Fig. 4 are the consequence of positioning the thermocouple at the fringes of the flame to avoid interferences with the multipass laser beam. The absolute water density accuracy compared to equilibrium predictions is better than 6%, and the precision is better than 1% for strongly absorbing conditions.

Integration Engineering for Scramjet Test Facility

The sensor was engineered for integration with the high-enthalpy flow facility at the U.S. Air Force Laboratory (AFRL) test cell 22 at Wright–Patterson Air Force Base. The sensor electronics package located in the facility control room was computer controlled and mounted in a standard half-height equipment rack. All laser control hardware, fiber optic splitters, data acquisition boards, etc., were mounted within the computer chassis. An ethernet board provided for periodic CPU clock calibration to a National Institutes of Standards and Technology atomic clock via internet access. System control was facilitated through LabView software routines. Fiber optic cables transported laser light to the supersonic combustion section of the model scramjet, and electrical cables transported detector signals back to the computer for analysis.

The design and engineering of the optical interface to the supersonic combustor is critical for high-temperature applications. Because the steady-state wall temperature of the combustor can exceed 400 K, it was necessary to cool the optics to protect the fiber optic collimators and InGaAs photo detectors. To achieve high absorbance sensitivity, the windows required anti-reflection coatings at the laser wavelength, and these coatings were limited to 500 K. In addition, particulate deposition on the windows was a concern. These considerations required the use of both water cooling and gaseous nitrogen film cooling to protect the optics. Because the flowfield was supersonic, minimizing flow perturbations due to the film cooling was critical for the design.

A schematic of the film cooling system is shown in Fig. 6. The IR-grade fused silica windows are 1.9 cm in diameter with a 2.54-cm-diam shoulder. The windows are AR-coated at 1.31 μm for an incidence angle of 15 deg. Nitrogen was fed through machined passages in the window mount and limited by a choked, 2.0-mm orifice. Mass flow for film cooling corresponded to about 5 standard cubic feet per minute (scfm) per window or 25 scfm, total, which was less than 0.5% of the main combustor flow.

Installation on the supersonic combustion tunnel (shown schematically in Fig. 7) required custom side wall panels to accommodate our optical mounts and their water and nitrogen gas cooling lines.

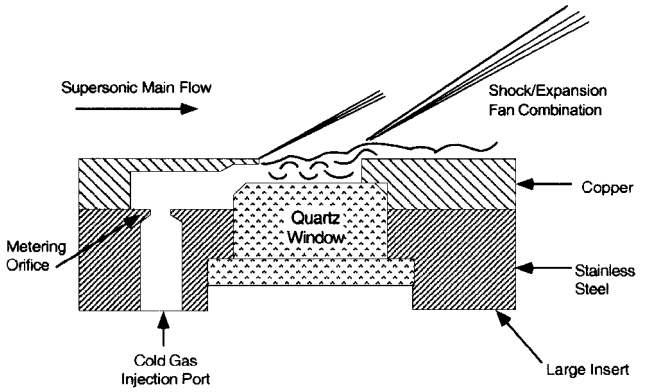

Fig. 6 Schematic of gaseous nitrogen film cooling system.

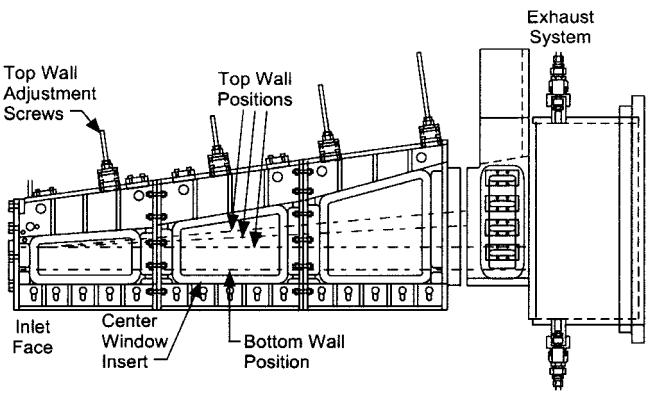

Fig. 7 Schematic of model scramjet combustor.

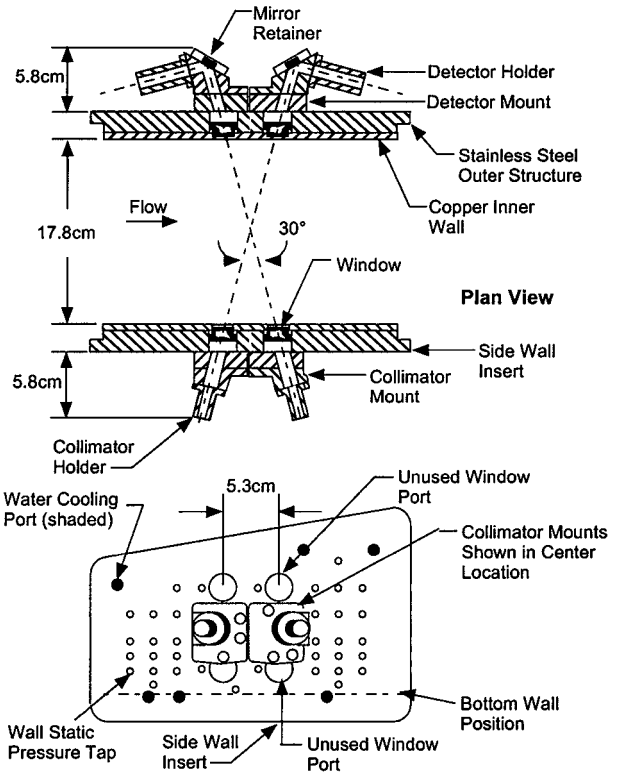

Fig. 8 Detailed schematics of optical integration hardware.

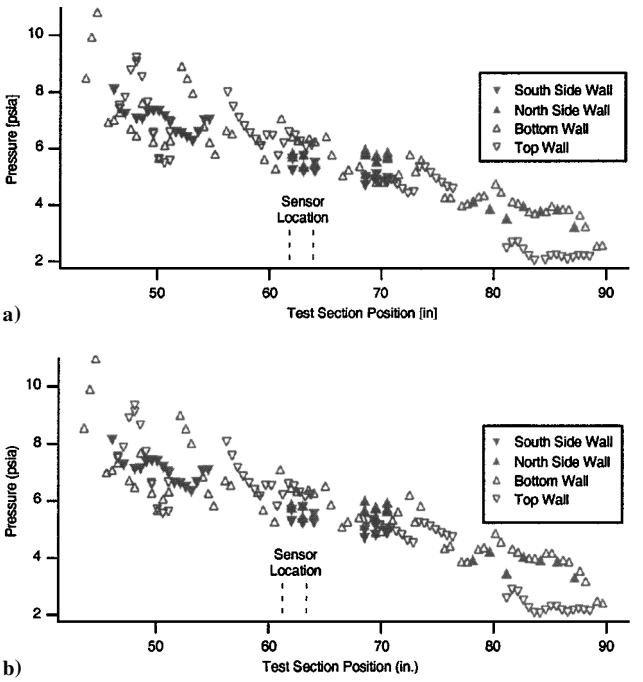

Fig. 9 Wall static pressure measurements along the combustor a) without and b) with window film cooling flow.

Flow in the tunnel test section schematic is from left to right, and the tunnel test section is immediately downstream of the expansion nozzle. The test section includes a variable expansion plate in the top. The side wall panels were positioned in the center corresponding to expanded conditions of Mach 2.1 at the sensor location. These panels, shown schematically in Fig. 8, indicate connections for water cooling, nitrogen gas film cooling, and a variety of locations for pressure taps to monitor potential flow disturbances. Water cooling to stabilize the panel for the optical windows required the removal of 200 W of thermal power and corresponded to an 11-K temperature rise for a nominal water flow rate of 8 gal/min with a pressure drop of 10 psi for each panel.

The detector holders for the sensor were purposely positioned after a turning mirror to reduce light collection by the detector from the heated walls and hot particles in the flowing gas stream. The mirrors possess a narrowband coating for maximum reflectivity only at the laser wavelength, further reducing the radiative load on the photodetectors. The collimating optics consisted of a 5-mm-diam antireflection coated asphere mounted directly onto the end of the fiber by the manufacturer. Typical collimated beam diameters from single-mode near-IR fibers are about 2 mm. No attempt was made in this setup to further expand this beam, although it is well known that increasing the beam diameter will reduce the angular deflection of a collimated light beam in the presence of a given density distortion. The beams impinged directly onto the largest area InGaAs photodetectors presently available with a 5-mm-diam active area.

Combustor Tests and Results

Preliminary tests on the combustor were performed without windows, fiber optics, or photodetectors. Fused silica windows were replaced with steel window blanks instrumented with thermocouples. These tests were used to evaluate cooling behavior of the custom panels and to monitor the tunnel for any flow disturbances generated by the gaseous nitrogen film cooling flow. The combustor inlet air was heated with a vitiated heater burning JP-4. Two expanded static pressure conditions were tested: 13 and 6 psia (0.88 and 0.41 atm). Stagnation temperatures at these conditions were set to 944, 1111, and 1250 K, corresponding to predicted freestream static temperatures at the sensor location of 540, 650, and 740 K.

Tests were performed with the maximum nitrogen film cooling to evaluate potential flow disturbances. Figure 9 shows wall pressure distributions with (Fig. 9a) and without (Fig. 9b) maximum nitrogen film cooling. The vertical dashed lines show the location of the sensor. No significant flow disturbances due to film cooling flow are evident in these data.

Thermocouples were monitored at several locations on the panel and at the steel replacement window. The maximum temperature recorded at any location on the panel or window insert was 341 K, which is well below the operating limit of 523 K imposed by the window coatings. At the highest stagnation temperature, 1250 K, the water flow increased temperature by 11 K between the inlet and outlet to the custom panel. A review of the steel window inserts was performed after the test runs. The steel windows inserts exhibited some contamination aligned with the flow direction and beginning about halfway across the steel window insert. Much of the contamination is expected to have accumulated during periods with no film cooling.

Several spectrally resolved lineshapes were obtained during the startup sequence and initial pumpdown of the tunnel. Figure 10a shows the atmospheric water absorption on the 7612 cm^{-1} doublet prior to pump down. The minimum tunnel pump down pressure is 3 psia (0.2 atm) and the observed water absorption at the 7612 cm^{-1} doublet under these conditions is shown in Fig. 10b. The narrow linewidths due to reduced collisional broadening are consistent with the low-pressure condition. At this low signal level, some optical interference fringe effects are evident in the baseline.

Simultaneous density, temperature, and velocity measurements were recorded at 1 Hz throughout the sequence of increasing stagnation temperatures at an expanded pressure of 13 psia. Figure 11 shows the measured water density during the sequence of changing stagnation temperatures. Figure 12 shows the simultaneous freestream static temperature measurement, and Fig. 13 the simultaneous velocity measurement.

The data exhibit the best signal to noise in the density measurement with decreasing signal to noise in the temperature measurement and large excursions in the velocity measurement. This behavior is nominally understood by recognizing that four different absorption lines are monitored, integrated, and averaged to determine density. The temperature measurement requires at least one line of sight in the high-speed flow to provide good signal to noise data so that the ratio of integrated absorption can be measured to determine the temperature. The temperature measurement exhibits the combined noise from both integrated lineshapes. The most demanding

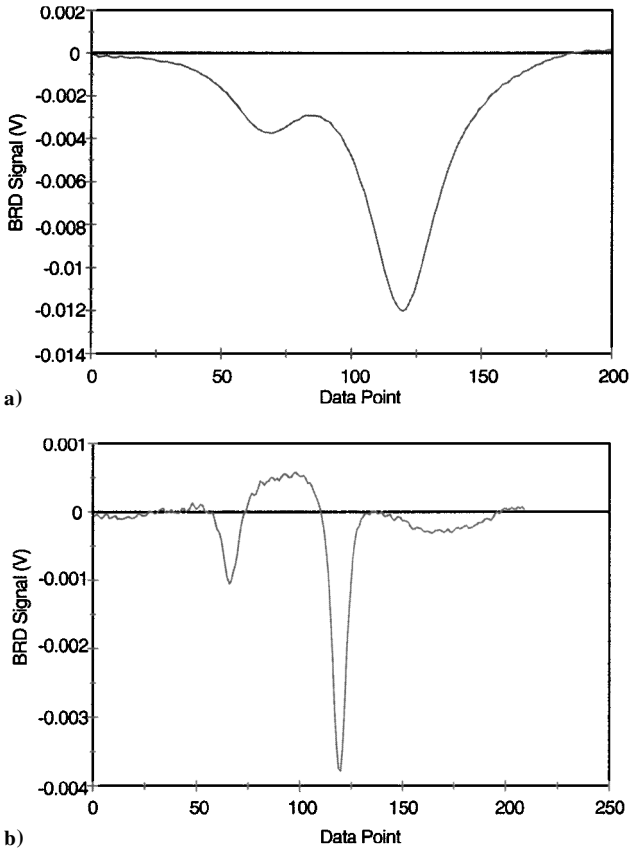

Fig. 10 Example water vapor lineshape at 7612 cm^{-1} with static ambient air in the a) combustor and b) after tunnel pump down.

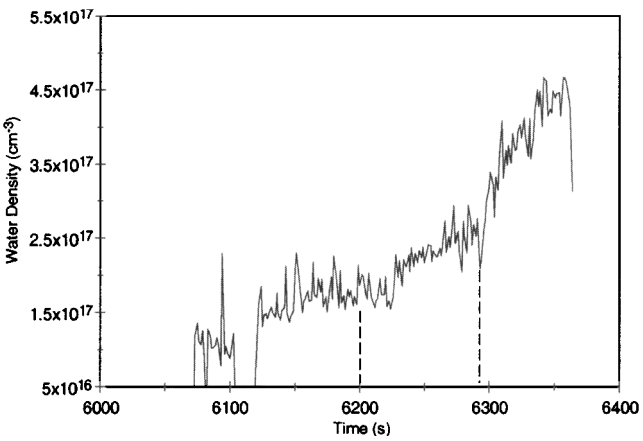

Fig. 11 Water density measurements during a sequence of changing stagnation temperatures.

is the velocity measurement, which requires high signal to noise in the lineshape to determine position shift, that is, not an integrated area, and requires that high signal to noise lineshapes be present on both lines of sight simultaneously. Further, the algorithms used to determine velocity are more sensitive to noise than either the density or temperature.[13]

Table 2 presents a summary of the measured and estimated conditions in the combustor at the sensor line of sight based on available flow models at AFRL. Although large excursions in the sensor output were observed, the optical sensor tracks both the water density and temperature changes. Note the vertical dashed lines in Figs. 11 and 12 indicate the beginning of 8-min time frames over which the stagnation conditions were held at a nominally steady test point. The sensor density and temperature measurements both suggest that the static conditions in the supersonic test section are not stable, but drift upward in density and temperature during these periods. At present, this effect is not well understood, but it is tentatively attributed to in-

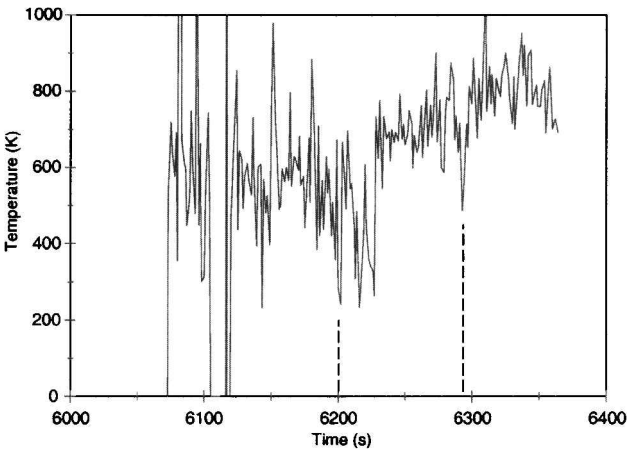

Fig. 12 Temperature measurements during the sequence of stagnation temperatures compared to predicted static values.

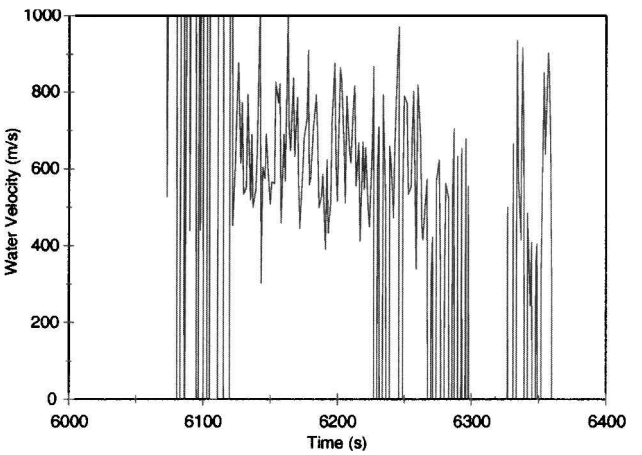

Fig. 13 Velocity measurements during the sequence of stagnation conditions.

stability in the facility operation. The measured water density shows a discrepancy with predictions ranging from 17 to 56% but has a precision of better than 10%. The present flow models used to predict the in-stream values should be considered as estimates at the present time, and more detailed model/experimental data comparisons are required before any concrete conclusions can be drawn regarding the absolute validity of either measurement or model. At this stage of the sensor development, we are more concerned with the precision of the sensor because that is an independent assessment of the stability of measurement condition. The measured temperatures show the best accuracy relative to predictions, 7–11%, but the low signal to noise results in temperature precisions of only ±100 K. The velocity measurement is the most distorted. The poor signal to noise in the velocity measurement is attributed to beam steering effects in the flow.

Analysis of the absorption lineshapes indicates several areas for improvement. Lineshapes of the two water absorptions at time 6351 s corresponding to the highest stagnation temperature are shown in Fig. 14. The signal to noise in the 7612-cm^{-1} absorption (Fig. 14a) is relatively good; however, the nonlinear baseline, especially in the wings of the absorption, may be interfering with the water absorption measurement. The common combustion products CO, CO_2, OH, NO, and NO_2 do not absorb in this region, but the absorption spectra of unburned JP-4 fuel and fuel fragments are not well documented at these conditions and may be contributing to some distortions in the baseline. The lower signal to noise in the 7632-cm^{-1} absorption line (Fig. 14b) arises from the weaker absorption strength of this feature and demonstrates the source of the lower signal-to-noise ratio in the temperature data as compared to the density data. Table 3 presents a summary of the lineshape parameters for these transitions. The predicted and measured lineshape parameters

Table 2 Summary of optical measurements and results

Condition	Stagnation pressure, psia	Expanded static pressure, psia	Stagnation temperature, R/K[a]	Predicted[a] expanded static temperature, K	Measured expanded static temperature, K	Predicted[a] water fraction, %	Measured water fraction, %	Predicted[a] flow velocity, m/s	Measured flow velocity, m/s
1	112	13	1700/944	540 ± 20	600 ± 100	2.5 ± 0.2	1.6 ± 0.16	970 ± 25	700 ± 100
2	112	13	2000/1111	650 ± 25	700 ± 100	3.8 ± 0.3	2.6 ± 0.26	1060 ± 30	——
3	112	13	2250/1250	740 ± 30	800 ± 100	4.8 ± 0.4	5.6 ± 0.56	1130 ± 35	——

[a]Estimated by AFRL at Mach = 2.1.

Table 3 Measured and predicted absorption line parameters for test conditions of 4.8% H_2O, 740 K, and 13 psia

	Line 1, 7612 cm^{-1}		Line 2, 7632 cm^{-1}	
Parameter	Prediction	Measurement	Prediction	Measurement
α Peak, cm	1.22×10^{-3}	$(1.12 \pm 0.22) \times 10^{-3}$	6.36×10^{-4}	$(1.3 \pm 0.2) \times 10^{-3}$
$\int \alpha \, d\nu$	2.64×10^{-4}	$(3.1 \pm 1.4) \times 10^{-4}$	1.17×10^{-4}	$(1.65 \pm 0.2) \times 10^{-4}$
$\Delta \nu$ FWHM, cm^{-1}[a]	0.110	0.106	0.093	0.089

[a]Full width at half-maximum.

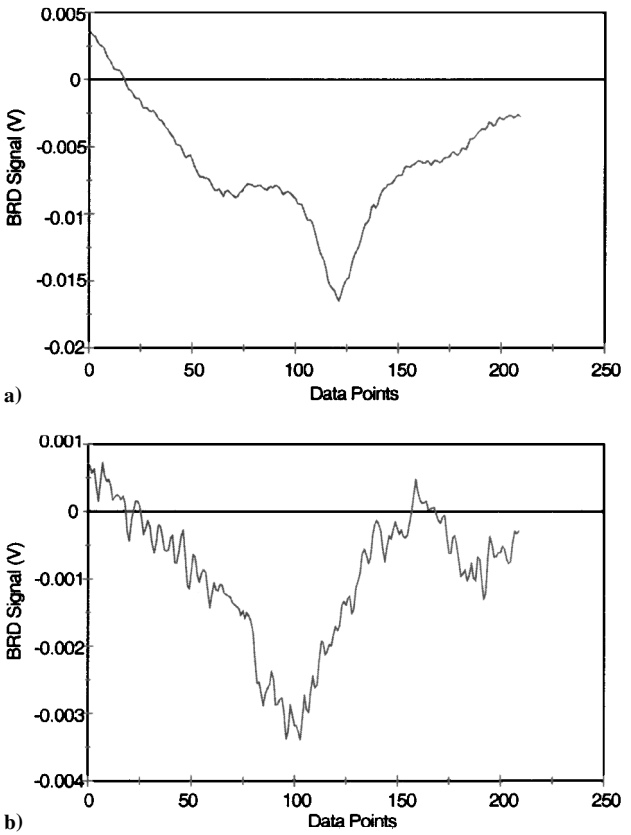

Fig. 14 Comparison of example water vapor line shapes at test time 6351 s at a) 7612 cm^{-1} and b) 7632 cm^{-1}.

are in relatively good agreement considering the signal to noise in the measured lineshapes. This result lends confidence in the conclusion that at these wavelengths relatively accurate measurements of water vapor are possible, even in such an extreme environment.

Discussion

Several conclusions can be drawn from these measurements. Most important is that optical hardware/installations and sensor techniques have matured to the point where nonintrusive measurements can be performed continuously on high-enthalpy combustion facilities. These measurements demonstrate technology to integrate sensitive fiber optic components, coated optical windows, and photodetectors that will survive extreme gas and facility temperature excursions.

In more benign laboratory environments, the sensors performed very well throughout the temperature range from 500 to 2100 K, where they provide water vapor density and temperature measurement accuracy and precision comparable to those of intrusive probe techniques. Water vapor density and temperature measurements in the model scramjet combustor were hindered by low signal to noise in the absorption lineshapes, yet tracked changes as the supersonic flow static conditions and the stagnation conditions were changed.

The velocity measurement is the simplest calculation and yet most demanding for the optical system. The sensor can obtain a density and temperature if either line of sight records a measurable absorption signal. The velocity measurement requires that both lines of sight see measurable absorptions with high signal to noise. Based on observations of the total transmitted power, we believe that the second line of sight was viewing through a fluctuating density gradient that caused the laser beam to steer off the detector on the opposite side panel. This density gradient could have been induced by the film cooling on one of the windows. Additional tests will be required to confirm this hypothesis and to correct the problem.

Several suggestions arise for improving the measurement. Increasing the magnitude of the absorption would improve the signal to noise. The selected lines may be more appropriate for a H_2 fueled combustor, but appear weak for the level of water generated by the JP-4 fueled heater. The peak absorption levels in theses test were on the order of $5–10 \times 10^{-4}$. Stronger water transitions near 7181 cm^{-1} (1.3925 μm) would result in peak absorption levels on the order of 10^{-1}, resulting in better signal to noise. In flows with water vapor content in excess of 20%, however, these strong lines may become optically thick (such a condition was an initial motivation for our choice of 1.31 μm). Larger pathlengths would serve the same purpose, although folded or multiple reflection optical path alignment may be problematic in such a demanding flow environment.

Conclusion

A sensor system using near IR diode lasers at 1.31 μm has been developed for simultaneous water density, temperature, and velocity measurements in advanced aeropropulsion test facilities. The nonintrusive line-of-sight absorption techniques used by the sensor were extensively tested in the laboratory. High-temperature absorption cell and flame studies were performed throughout the temperature range from 500 to 2000 K. Absorption measurements were calibrated using available spectroscopic databases, flame chemistry modeling, and a variety of laser diagnostics. Laboratory performance with a 0.3-Hz bandwidth indicated density accuracy of better than 10%, from 10^{16} to 10^{19} cm^{-3}, a temperature accuracy of 5%, from 500 to 2000 K, and a velocity accuracy of better than 5%.

The sensor was installed on the model scramjet combustor at the AFRL at Wright–Patterson Air Force Base. Sensor agreement with predictions ranged from 17 to 56% for water density measurements and from 7 to 11% for the temperature measurements.

Further improvements require better matching of the absorption linestrengths to expected water concentration conditions.

Additional, further engineering is required to verify the severity of beam steering and to develop solutions to mitigate this influence, such as large area beams and focusing systems.

Acknowledgments

This work was supported by the AFRL under Contract F33615-95-C-2562. We wish to thank Kevin Jackson and Mark Gruber of AFRL as well as the entire crew of test cell 22 for their support in completing these measurements and providing estimates of expected flow parameters for comparison.

References

[1]Park, C., "Evaluation of Real-Gas Phenomena in High-Enthalpy Impulse Test Facilities: A Review," *Journal of Thermophysics and Heat Transfer*, Vol. 11, No. 1, 1997.

[2]Dunn, M. G., "Experimental Study of High-Enthalpy Shock-Tunnel Flow, Part II: Nozzle-Flow Characteristics," *AIAA Journal*, Vol. 7, No. 9, 1969, pp. 1717–1723.

[3]Upschulte, B. L., Allen, M. G., and McManus, K. R., "Fluorescence Imaging of NO, O_2 in a Spray Flame Combustor at Elevated Pressures," *Twenty-Sixth Symposium (International) on Combustion*, Combustion Inst., Pittsburgh, PA, 1996, pp. 2779–2786.

[4]Upschulte, B. L., Allen, M. G., and Sonnenfroh, D. M., "Measurements of CO, CO_2, OH, and H_2O in Room Temperature and Combustion Gases by Use of a Broadly Current-Tuned Multi-Section Diode Laser," *Applied Optics*, Vol. 38, No. 9, 1999, pp. 1506–1512.

[5]Allen, M. G., Parker, T. E., Reinecke, W. G., Legner, H. H., Foutter, R. R., Rawlins, W. T., and Davis, S. J., "Fluorescence Imaging of OH and NO in a Model Supersonic Combustor," *AIAA Journal*, Vol. 31, No. 3, 1993, pp. 505–512.

[6]Parker, T. E., Allen, M. G., Reinecke, W. G., Legner, H. H., Foutter, R. R., and Rawlins, W. T., "High Temperature Supersonic Combustor Testing with Optical Diagnostics," *Journal of Propulsion and Power*, Vol. 9, No. 3, 1993, p. 486.

[7]Allen, M. G., Davis, S., Kessler, W., Legner, H., McManus, K., Mulhall, P., Parker, T., and Sonnenfroh, D., "Velocity Field Imaging in Supersonic Reacting Flows near Atmospheric Pressure," *AIAA Journal*, Vol. 32, No. 8, 1994, pp. 1676–1682.

[8]Verdieck, J., Yang, T. T., Burde, D., and Allen, M., "PLIF Diagnostics for Scramjet Engine Concept Testing," Paper No. 235, 10th National Aerospace Plane Symposium, NASA, April 1991.

[9]Roberts, W. L., Allen, M. G., Howard, R. P., Wilson, G., and Trucco, R., "Measurement of Nitric Oxide in the HYPULSE Expansion Tube Facility," AIAA Paper 94-2644, 1994.

[10]Baer, D. S., Nagali, V., Furlong, E. R., Hanson, R. K., and Newfield, M. E., "Scanned- and Fixed-Wavelength Absorption Diagnostics for Combustion Measurements Using Multiplexed Diode Lasers," *AIAA Journal*, Vol. 34, No. 3, 1996, pp. 489–493.

[11]Furlong, E. R., Baer, D. S., and Hanson, R. K., "Combustion Control Using a Multiplexed Diode-Laser Sensor System," *Twenty-Sixth Symposium (International) on Combustion*, Combustion Inst., Pittsburgh, PA, 1996, pp. 2851–2858.

[12]Allen, M. G., and Kessler, W. J., "Simultaneous Water Vapor Concentration and Temperature Measurements Using 1.31-μm Diode Lasers," *AIAA Journal*, Vol. 34, No. 3, 1996, pp. 483–488.

[13]Miller, M. F., Kessler, W. J., and Allen, M. G., "Diode Laser-Based Air Mass Flux Sensor for Subsonic Aeropropulsion Inlets," *Applied Optics*, Vol. 35, No. 24, 1996, pp. 4905–4912.

[14]Sonnenfroh, D. M., and Allen, M. G., "Measurements of the Second Overtone Absorption Band of NO in Ambient and Combustion Gases Using a 1.8 Micron, Room Temperature Diode Laser," *Applied Optics*, Vol. 36, 1997, pp. 7970–7977.

[15]Allen, M. G., "Diode Laser Absorption Sensing of Gas Dynamic and Combustion Flows," *Measurement Science and Technology*, Vol. 9, No. 4, 1998, pp. 545–562.

[16]Wehe, S. D., Baer, D. S., Hanson, R. K., and Chadwick, K. M., "Measurements of Gas Temperature and Velocity in Hypervelocity Flows Using a Diode-Laser Absorption Sensor," AIAA Paper 98-2699, June 1998.

[17]Wehe, S. D., Baer, D. S., and Hanson, R. K., "Tunable Diode-Laser Absorption Measurements of Temperature, Velocity, and H_2O in Hypervelocity Flows," AIAA Paper 97-3267, July 1997.

[18]Mohamed, A., Rosier, B., Henry, D., Louver, Y., and Varghese, P. L., "Tunable Diode Laser Measurements on Nitric Oxide in a Hypersonic Wind Tunnel," *AIAA Journal*, Vol. 34, No. 3, 1996, pp. 494–499.

[19]Jackson, K., Gruber, M., Mathur, T., Streby, G., Smith, C., and Billig, F., "Calibration of Newly Developed Direct-Connect High Enthalpy Supersonic Combustion Research Facility," AIAA Paper 98-1510, April 1998.

[20]Hobbs, P. C. D., "Ultrasensitive Laser Measurements Without Tears," *Applied Optics*, Vol. 36, No. 4, 1997, pp. 903–920.

[21]Allen, M. G., Carleton, K. L., Davis, S. J., Kessler, W. J., Otis, C. E., Palombo, D. A., and Sonnenfroh, D. M., "Ultra-Sensitive Dual-Beam Absorption and Gain Spectroscopy: Applications for Near-IR and Visible Diode Laser Sensors," *Applied Optics*, Vol. 34, No. 18, 1995, pp. 3240–3249.

[22]Rothman, L. S., Gamache, R. R., Tipping, R. H., Rinsland, C. P., Smith, M. A. H., Benner, D. C., Devi, V. M., Flaudt, J.-M., Camy-Peyret, A., Goldman, A., Massie, S. T., Brown, L. R., and Toth, R. A., "The HITRAN Molecular Database: Editions of 1991 and 1992," *Journal of Quantitative Spectroscopy and Radiative Transfer*, Vol. 48, 1993, pp. 469–507.

[23]Rothman, L. S., Wattson, R. B., Gamache, R. R., Goorvetch, D., Hawkins, R. L., Selby, J. E. A., Camy-Peyret, C., Flaud, J.-M., Schroeder, J., and McCann, A., "HITEMP, the High-Temperature Molecular Spectroscopic Database," *Journal of Quantitative Spectroscopy and Radiative Transfer* (to be published).

[24]Upschulte, B. L., and Allen, M. G., "Diode Laser Measurements of Line Strengths and Self-Broadening Parameters of Water Vapor Between 300 and 1100 K Near 1.31 μm," *Journal of Quantitative Spectroscopy and Radiative Transfer*, Vol. 59, No. 6, 1998, pp. 653–670.

[25]Kessler, W. J., Allen, M. G., and Davis, S. J., "Rotational Level-Dependent Collisional Broadening and Line Shift of the $A^2\Sigma^+$-$X^2\Pi$ (1, 0) Band of OH in Hydrogen–Air Combustion Gases," *Journal of Quantitative Spectroscopy and Radiative Transfer*, Vol. 49, No. 2, 1993, p. 107.

[26]Herriott, D. R., and Schulte, H. J., "Folded Optical Delay Lines," *Applied Optics*, Vol. 4, No. 8, 1965, pp. 883–889.

[27]Bradley, D., and Entwhistle, A. G., "Determination of the Emissivity for Total Radiation of Small Diameter Platinum—10% Rhodium Wires in the Temperature Range 600 to 1450°C," *British Journal of Applied Physics*, Vol. 12, 1961, p. 708.

[28]Grosshandler, W. L., Engle, M., and Russell, A., "Emissivity of Thermocouples for Combustion Measurements," Combustion Inst., Paper WSS/CI 80-21, April 1980.

R. P. Lucht
Associate Editor